YU.V. KOVTUN, E.I. SKIBENKO, A.I. SKIBENKO, V.B. YUFEROV

National Science Center Kharkiv Institute of Physics and Technology,
Nat. Acad. of Sci. of Ukraine
(1, Akademichna Str., Kharkiv 61108, Ukraine; e-mail: Ykovtun@kipt.kharkov.ua)

ROTATION OF PLASMA LAYERS WITH VARIOUS DENSITIES IN CROSSED E × B FIELDS

PACS 52.80.Sm; 52.65.Kj

The rotational velocity of plasma layers with various densities in a pulsed reflex-discharge plasma is studied with the use of the two-frequency microwave fluctuation reflectometry. The difference between the angular rotational velocities of plasma layers with different densities is revealed, and their time dependences are determined. The rotational velocity of plasma layers is found to increase with the magnetic field induction. On the basis of the experimental data obtained, the radial electric field strength in the plasma layers concerned is evaluated.

K e y w o r d s: plasma, fluctuation reflectometry, plasma layers.

1. Introduction

Experimental researches of plasma in crossed $\mathbf{E} \times \mathbf{B}$ fields were started at the beginning of the 1950s in the framework of the activity aimed at the controlled thermonuclear fusion [1–3], although the works dealing with gas discharges in crossed fields were initiated at the end of the 19th and the beginning of the 20th centuries [4–6]. Nowadays, the experiments devoted to various physical and applied aspects concerning the plasma in crossed fields are intensively carried out on various experimental installations, such as MCX [7], MISTRAL [8], MBX [9], ALEXIS [10], and a number of others. One of the features for plasma created and held in crossed $\mathbf{E} \times \mathbf{B}$ fields is its drift rotation. Under certain conditions, various instabilities can develop in the rotating plasma, which may bring about, e.g., the heating of the plasma ion component [11, 12]. In the case of multicomponent plasma, the rotation of a plasma column gives rise to the spatial separation of the ion component [13]. There can be several variants at that. First, plasma contains ions with identical masses, but in different charged states. In this case, ions with a large Z drift toward the center of the plasma column. Second, plasma contains ions with different masses. In this case, owing to centrifugal forces that arise in the rotating plasma, the ions become radially separated according to their masses. The third variant, in essence, is a combination of the first and second ones. The efficiency of the radial ion separation depends on the rotational velocity [13]. In connection with the aforesaid, the determination of the plasma rotational velocity is of a certain interest. On the other hand, the experimental research of the rotational velocity in plasma was carried out mainly for the plasma of various gases or their mixtures [14, 15], as well as the gas-metal plasma [16]. The study of rotation in a gas-metal plasma has the pure physical importance, as well as the applied significance.

Therefore, this work is aimed at studying the rotational velocity in the multicomponent gas-metal plasma embedded in crossed $\mathbf{E} \times \mathbf{B}$ fields. It continues our earlier researches of a multicomponent gas-metal plasma created in the pulsed reflex discharge [17–21].

2. Plasma Motion in Crossed E × B Fields

In the non-relativistic case, the equation of motion for a charge in an electromagnetic field looks like [22, 23]

$$m\frac{d\mathbf{v}}{dt} = q\mathbf{E} + q\,[\mathbf{v} \times \mathbf{B}], \qquad (1)$$

where $\mathbf{E} = -\frac{1}{c}\frac{d\mathbf{A}}{dt} - \bigtriangledown\phi$ is the electric field strength, $\mathbf{B} = \text{rot}\ \mathbf{A}$ the magnetic field induction, $q = Ze$ the ion charge, e the elementary charge, m the particle's mass, $\mathbf{A}$ the vector potential of the field, $\mathbf{v}$ the particle's velocity, and ϕ the scalar potential of the field. The motion of a charged particle in crossed electric and magnetic fields, in particular, in an axially symmetric reflex discharge, is described by the following system of differential equations (in the cylindrical coordinates):

$$\begin{cases} m\left(\ddot{r} - r\dot{\varphi}^2\right) = qE_r + qr\dot{\varphi}B_z, \\ m\dfrac{1}{r}\dfrac{d}{dt}\left(r^2\dot{\varphi}\right) = q\left(\dot{z}B_r - \dot{r}B_z\right), \\ m\ddot{z} = qE_z - qr\dot{\varphi}B_r. \end{cases} \tag{2}$$

For the state equilibrated in the radial direction, the first equation of system (2) looks like

$$mr\omega^2 + qr\omega B_z + qE_r = 0, \tag{3}$$

where $\dot{\varphi} = \omega$ is the angular velocity. As is seen from Eq. (3), the particle is subjected to the action of the following forces in the radial direction perpendicular to the particle rotation axis: (i) the centrifugal force associated with particle's motion, $mr\omega^2$; (ii) the magnetic force associated with the action of magnetic field on the particle, $qr\omega B_z$; and (iii) the electric force produced by the electric field, qE_r. The drift of the particle is determined by the relation [1]

$$v_{i\varphi} = -\frac{E_r}{B_z} - \frac{m_i v_{i\varphi}^2}{rqB_z},$$

where $v_{i\varphi} = \omega r$ is the rotational velocity. The solution of the quadratic equation (3) for ions with regard for the particle charge and the field direction (it is directed radially toward the rotation axis, so that the positive potential increases with the distance to the rotation axis) reads

$$v_{i\varphi} = \frac{\Omega_i r}{2}\left(-1 + \sqrt{1 + \frac{4E_r}{rB_z\Omega_i}}\right), \tag{4}$$

where $\Omega_i = \frac{qB_z}{m_i}$ is the Larmor frequency of ion rotation, r the rotation radius, and m_i the ionic mass. For an electron, the centrifugal force $mr\omega^2$ is small and, hence, can be neglected. Then, the rotational velocity equals

$$v_{e\varphi} = \frac{E_r}{B_z}. \tag{5}$$

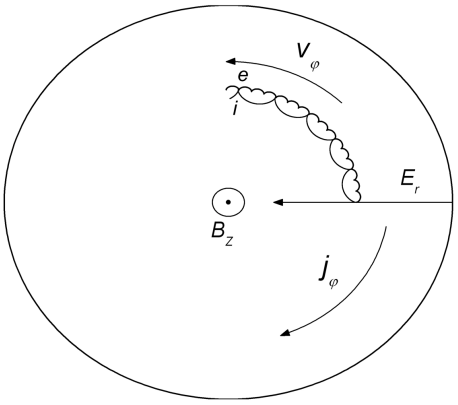

Fig. 1. Rotation of electrons e and ions i in crossed $\mathbf{E} \times \mathbf{B}$ fields

Owing to the difference between the rotational velocities v_φ for electrons and ions, there emerges a circular electric current, with its density being proportional to the difference between the corresponding values for both plasma components [1].

$$j_\varphi = Nq\left(v_{i\varphi} - v_{e\varphi}\right). \tag{6}$$

The current induces the diamagnetic effect and diminishes the magnetic field induction in plasma, in addition to a reduction associated with the usual plasma diamagnetism. As an illustration of the aforesaid, Fig. 1 exhibits the trajectories of particles and the direction of their rotation in the crossed $\mathbf{E} \times \mathbf{B}$ fields.

In the framework of the macroscopic approach, the average velocity of all particles (of a certain kind) included into an element of volume is considered. Then, every plasma component can be regarded as a fluid, the motion of which is described by the macroscopic velocity. In the two-fluid magnetohydrodynamic (MHD) model, the equations of motion look like [24]

$$N_e m_e\left(\frac{d\mathbf{v}_e}{dt} + \left(\mathbf{v}_e\nabla\right)\mathbf{v}_e\right) = \\ = N_e q\left[\mathbf{E} + \mathbf{v}_e \times \mathbf{B}\right] - \nabla P_e + R, \tag{7}$$

$$N_i m_i\left(\frac{d\mathbf{v}_i}{dt} + \left(\mathbf{v}_i\nabla\right)\mathbf{v}_i\right) = \\ = N_i q\left[\mathbf{E} + \mathbf{v}_i \times \mathbf{B}\right] - \nabla P_i - R, \tag{8}$$

where N_e and N_i are the concentrations of electrons and ions, respectively; m_e and m_i are the masses of

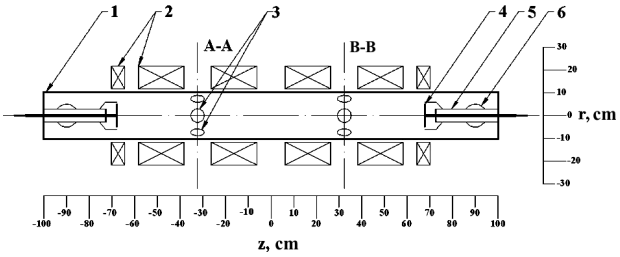

Fig. 2. Diagram of the pulsed reflex-discharge installation: (*1*) discharge chamber (anode), (*2*) magnetic system, (*3*) diagnostic ports, (*4*) cathodes, (*5*) insulator, (*6*) vacuum pumping system, (A–A and B–B) cross-sections of the diagnostic port arrangement

electron and ion, respectively; $\mathbf{v}_e$ and $\mathbf{v}_i$ are the velocities of electrons and ions, respectively; P_e nad P_i are the pressures of the electron and ion components, respectively; $R = -N_e m_e (\mathbf{v}_e - \mathbf{v}_i) \nu_{ei}$ is the friction force; and ν_{ei} is the frequency of collisions between the electrons and ions. For the state equilibrated in the radial direction, from Eq. (8) and assuming $v_{ir} = v_{er} = 0$, we obtain that, for ions,

$$m_i r\omega^2 + qr\omega B_z + qE_r - \frac{1}{N_i}\nabla P_i = 0. \tag{9}$$

For electrons, a similar equation can be obtained. Equation (9) transforms to the form

$$v_{i\varphi} = -\frac{E_r}{B_z} - \frac{m_i v_{i\varphi}^2}{rqB_z} + \frac{1}{N_i q B_z} \bigtriangledown P_i. \tag{10}$$

Whence, one can see that the rotational velocity consists of the drift in the electric field, the centrifugal drift, and the diamagnetic drift. The solution of quadratic Eq. (9) with regard for the charge of an ion and the field direction looks like

$$v_{i\varphi} = \frac{\Omega_i r}{2}\left(-1 + \sqrt{1 + \frac{4E_r}{rB_z\Omega_i} + \frac{4\nabla P_i}{rm_i N_i \Omega_i^2}}\right). \tag{11}$$

For electrons, when the centrifugal force is neglected, we obtain

$$v_{e\varphi} = \frac{E_r}{B_z} - \frac{1}{N_e q B_z} \bigtriangledown P_e. \tag{12}$$

If the diamagnetic drift is not taken into account, Eqs. (11) and (12) look similarly to Eqs. (4) and (5), respectively.

In the one-fluid MHD model, the equation of motion for the plasma as a whole reads

$$\rho\left(\frac{d\mathbf{v}}{dt} + (\mathbf{v}\nabla)\,\mathbf{v}\right) = \mathbf{j}\times\mathbf{B} - \nabla P, \tag{13}$$

where $P = P_e + P_i$ is the total plasma pressure; ρ is the plasma mass density ($\rho \approx N_p m_i$, because $m_e \ll m_i$); $\mathbf{v} = N_p (m_i\mathbf{v}_i + m_e\mathbf{v}_e)/\rho$ is the velocity of the plasma charged component; and $\mathbf{j} = eN_p \times (\mathbf{v}_i - \mathbf{v}_e)$ is the current density ($N_i = N_e = N_p$). Decomposing Eq. (13), we obtain

$$\rho\left(\frac{dv_r}{dt} + v_r\frac{dv_r}{dr} - \frac{dv_\varphi^2}{r}\right) = j_\varphi B_z - \frac{dP}{dr}, \tag{14}$$

$$\rho\left(\frac{dv_\varphi}{dt} + v_r\frac{dv_\varphi}{dr} + \frac{v_\varphi v_r}{r}\right) = -j_r B_z. \tag{15}$$

No.	Parameter	Value
1	Discharge voltage, kV	$\leq$4.5
2	Discharge current, kA	$\leq$2
3	Current pulse duration, ms	$\leq$1
4	Capacitor bank, μF	560
5	Energy duty, kJ	≤ 6
6	Magnetic field induction, T	$\leq$0.9
7	Mirror ratio R	1.25
8	Vacuum chamber volume, cm^3	$\sim 6.6 \times 10^4$
9	Initial pressure, Pa	1.33×10^{-4}
10	Working pressure, Pa	0.133–4.7
11	Diameter of cathodes, cm	10
12	Cathode material	Ti
13	Ignition gas	Ar
14	Plasma volume, cm^3	$\sim 10^4$

3. Experimental Installation and Diagnostic Techniques

The rotational velocity of the gas-metal plasma created in a high-current pulsed reflex discharge was experimentally studied on an installation exhibited in Fig. 2. The gas-metal plasma was formed as a result of a discharge in an environment consisting of a working gas, Ar, and a sputtered material of cathodes. The cathodes were fabricated from monometallic Ti. The supply of the cathode material (Ti) into plasma was confirmed by spectrometric measurements [17–19], with the amount of titanium in plasma could be at a level of 40–50% [20]. The maximum plasma density amounted to $N_p \sim 10^{14}$ cm^{-3}. The main electrophysical parameters of the installation and the discharge are quoted in Table. A pulsed magnetic

field of the mirror configuration and 18 ms in duration was created by a solenoid composed of six coils (see Fig. 2). The time dependences of the magnetic field induction for various voltages U_B at a capacitor bank of the magnetic system are depicted in Fig. 3.

A variety of diagnostic techniques for the determination of a plasma rotational velocity are known. These are the corpuscular-optical (the charge-exchange spectroscopy), optical (the Doppler spectrometry), microwave (the Doppler and fluctuation reflectometry), and probe methods. The choice of that or another diagnostic technique is mainly associated with a possibility of its application under specific experimental conditions. To study the rotation in a multicomponent gas-metal plasma, the most suitable are contactless methods including the optical and microwave methods. Both methods have their specific advantages and shortcomings. The main advantage of the optical method consists in the capability of measuring the rotational velocity of different plasma ions, although rather a complicated hardware is required for this purpose – especially if the radial dependence of the rotational velocity is determined. Microwave methods are simple enough from this aspect; however, they allow the density and rotational velocity of only the electron plasma component to be determined. In this connection, we chose the method of microwave fluctuation reflectometry. This method is based on the determination of the auto- and cross-correlation functions for two poloidally separated microwave signals reflected from a plasma layer with the same density. The auto- and cross-correlation functions can be calculated by the formulas

$$c_{xx}(\tau_k) = \frac{1}{N}\sum_{t=0}^{N-1} x(t)\, x(t+\tau_k), \tag{16}$$

$$c_{xy}(\tau_k) = \frac{1}{N}\sum_{t=0}^{N-1} x(t)\, y(t+\tau_k), \tag{17}$$

where $c_{xx}(\tau_k)$ and $c_{xy}(\tau_k)$ are the auto- and cross-correlation, respectively, functions for the signals $x(t)$ and $y(t)$; N is the number of pixels in the $x(t)$- and $y(t)$-realizations; and τ_k is the time lag between two signals. In contrast to the measurements of the Doppler frequency shift for a microwave signal, when the sounding direction is inclined and the reflection points do not coincide with the layer where $N_p = N_{\text{cr.}}$, the correlation method is based on the normal sounding. Therefore, the spatial position of the layer and its rotational velocity can be determined simultaneously, which is especially important for diagnosing the pulsed discharge plasma. In the case of a profile with the circular symmetry, the velocity of poloidal plasma rotation is found from the relation

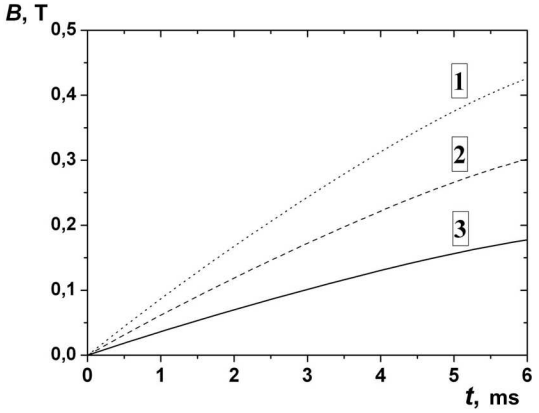

Fig. 3. Time dependence of the magnetic field induction. $U_B = 2$ (*1*), 1.4 (*2*), and 0.84 kV (*3*)

$$v_\varphi = \frac{\Delta l}{\Delta t} = \frac{\Delta\varphi r}{\Delta t}, \tag{18}$$

where $\Delta\varphi$ is the angular distance between the points of the reflected wave detection, r is the position of the reflecting layer determined from the phase shift of a reflected wave; and Δt is either the shift of the cross-correlation function (CCF) maximum in time or the period of the auto-correlation function (ACF).

One of the features of this work consists in the application of two-frequency microwave fluctuation reflectometry for the determination of the rotational velocity of plasma layers with $N_p = N_{\text{cr.}}^{1,2}$ in the reflex discharge. The plasma sounding frequency was so selected that, firstly, a layer with $N_p = N_{\text{cr.}}^{1,2}$ should exist in the generated plasma, and, secondly, plasma layers with different $N_{\text{cr.}}^{1,2}$ should be separated from each other by a distance that is larger than the uncertainty in the position of the reflecting layer [25]. Therefore, two sounding frequencies were selected, $f_1 = 37.13$ GHz and $f_2 = 72.88$ GHz, which corresponded to $N_{\text{cr.}}^1 = 1.7 \times 10^{13}$ cm^{-2} and $N_{\text{cr.}}^2 = 6.5 \times 10^{13}$ cm^{-3}, respectively. The plasma was sounded using an ordinary (O) wave across the plasma column and in the same cross-section for both frequencies. The arrangement diagram for microwave

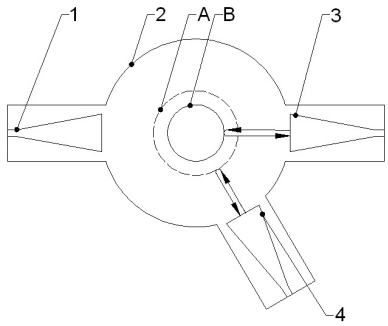

Fig. 4. Diagram of the arrangement of antennas for correlation and interferometric measurements: (*1*) receiving antenna of interferometer, (*2*) vacuum chamber, (*3* and *4*) transmit-receive antennas of a reflectometer. **A** and **B** are plasma layers with $N_p = N_{\text{cr.}}^{1,2}$

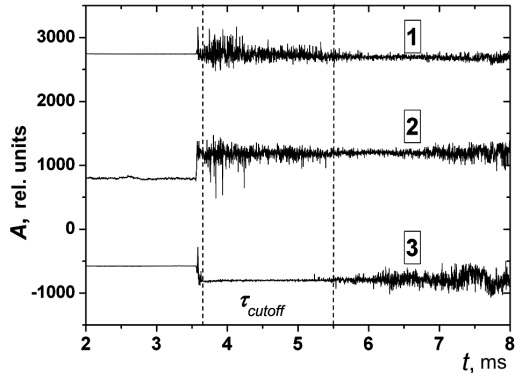

Fig. 5. Oscillograms of signals reflected from plasma layers with $N_p = N_{\text{cr.}}^1 = 1.7 \times 10^{13}$ cm^{-3} (*1* and *2*) and the signal from a UHF-interferometer, $\lambda = 8$ mm (*3*)

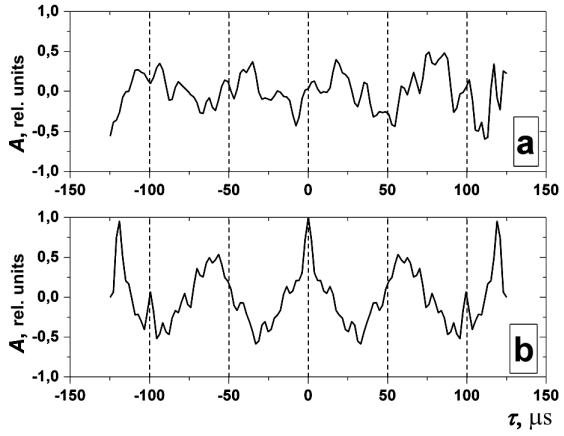

Fig. 6. Cross-correlated (*a*) and auto-correlated (*b*) functions for a reflected signal

antennas is shown in Fig. 4. The application of two combined antennas poloidally separated by an angle of 60° enabled the ACF and CCF to be used depending on the scheme of antenna connection; i.e. each of the antennas was used only for one sounding frequency, or both antennas were simultaneously supplied with microwave signals of different frequencies. Simultaneously with reflectometric measurements, the maximum, $N_p = N_{\text{cr.}}^{1,2}$, and average densities were measured with the help of an UHF interferometer. It allowed us to determine the lifetime interval for the layer with the critical density. The signals were registered with the use of an analog-to-digital converter with a frequency of 20 MHz.

4. Experimental Results

The rotational velocity in the gas-metal plasma Ar + Ti was experimentally studied under the following initial conditions for the experimental installation (see Fig. 2): the initial discharge voltage $U_{\text{dis.}} = 3.8$ kV ($Q \approx 4$ kJ, $P \approx 4$ MW); the pressure of the ignition gas, Ar, $p = 0.8$ Pa ($N_0 \approx 2 \times 10^{14}$ cm^{-3}); the magnitude of magnetic field induction was set by establishing three values of voltage U_B at the capacitor bank of the magnetic system, $U_B = 0.85$, 1.4, and 2 kV (see Fig. 3).

Under those initial conditions, a gas-metal plasma with the density $N_p \sim 10^{14}$ cm^{-3} emerges in the discharge. This means that the plasma layers exist with $N_{\text{cr}}^1 = 1.7 \times 10^{13}$ cm^{-3} and $N_{\text{cr}}^2 = 6.5 \times 10^{13}$ cm^{-3}, which allowed us to use the sounding frequencies $f^1 = 37.13$ GHz and $f^2 = 72.88$ GHz. The times of the existence of plasma layers with $N_{\text{cr}}^1 = 1.7 \times 10^{13}$ cm^{-3} and $N_{\text{cr}}^2 = 6.5 \times 10^{13}$ cm^{-3}, which were determined with the help of an UHF interferometer – i.e. the times of the microwave signal cut-off τ_{cutoff} – equaled about 1.8 and 1 ms, respectively, at $U_B = 1.4$ kV [17]. Typical oscillograms of signals obtained from the UHF interferometer and UHF reflectometers are shown in Fig. 5. The behavior of ACF and CCF for the reflected signal is illustrated in Fig. 6.

The dynamics of a reflex-discharge plasma can be conditionally divided into a few stages [18, 19]. At the first stage, the plasma layers with $N_p = N_{\text{cr.}}^{1,2}$ and the radius equal to the sounding wavelength, $r = \lambda$, emerge. The second stage includes the presence of plasma layers with $N_p = N_{\text{cr.}}^{1,2}$. At this stage, the radial dimensions of plasma layers grow in time. In other words, the plasma layers move toward the

combined antennas of reflectometer (see Fig. 4), until their radius reaches a certain value $r = r_{\max}$. Then, the growth of plasma layers stops, and their radii practically do not change during the time interval Δt (hundreds of microseconds). Further, the radial dimensions of plasma layers diminish, and the third stage begins, when the density decreases and the plasma decays.

The character of the phase variation for two microwave signals (see Fig. 5) reflected from a plasma layer with uniform density and poloidally separated at two points (see Fig. 4) testifies that the phase shifts in different cross-sections at the same frequency are identical at a fixed time moment, which confirms the symmetry of a plasma column with respect to its axis. The maximum radius of plasma layers with the critical density $N_p = N^{1,2}_{\text{cr.}}$ grows with the initial magnetic field and, at $B = 0.2$ T ($U_B = 2$ kV), reaches the values $r^1_{\max} \approx 5$ cm and $r^2_{\max} \approx 3.9$ cm for $N^1_{\text{cr}} = 1.7 \times 10^{13}$ cm^{-3} and $N^2_{\text{cr}} = 6.5 \times 10^{13}$ cm^{-3}, respectively.

The time dependences of the rotational velocities of plasma layers with $N_p = 1.7 \times 10^{13}$ cm^{-3} (layer **A**) and $N_p = 6.5 \times 10^{13}$ cm^{-3} (layer **B**) obtained for a number of discharge pulses are plotted in Fig. 7. Similar dependences were obtained for other values of magnetic induction as well. One can see that the rotational velocity grows to a certain value and then starts to fall down, with the maximum velocity being observed at the radius $r = r_{\max}$. The angular rotational velocities ω_φ for layers **A** and **B** with different radii are also different, i.e. $\omega^{\text{A}}_\varphi \neq \omega^{\text{B}}_\varphi$.

In Fig. 8, the dependences of the maximum rotational velocity $v_{\max}$ on the magnitude of initial magnetic field B are depicted. The dependences are increasing functions, i.e. the values of B and $v_{\max}$ grow together. When the velocity increases, the radii of layers with $N_p = N^{1,2}_{\text{cr.}}$ also increase, which was mentioned above. In this case, it is natural to assume that the velocity increases with the radius, because they are coupled by the relation $v_\varphi = \omega_\varphi r$ and may be independent, probably, of the magnetic field. However, as the radius increases, the growth of the angular velocity with B is also experimentally observed, which confirms, in essence, the growth of $v_{\max}$ with B.

5. Discussion of Experimental Results

Experimentally, the difference between the angular velocities of rotation for layers with $N_p = N^{1,2}_{\text{cr.}}$ was observed ($\omega^{\mathbf{A}}_\varphi \neq \omega^{\mathbf{B}}_\varphi$). If the plasma layers rotate as a whole (similarly to a solid body), the angular velocity ω_φ of rotation for layers with different radii would have been identical, and the linear velocity would have grown proportionally to the radius. At the same time, the results obtained testify that the model of plasma rotation as a whole is inapplicable in this case. Similar conclusions were made in work [14] devoted to studying a weakly ionized plasma of reflex discharge with the heated cathode.

The increase of the maximum rotational velocity $v_{\max}$ with the growth of B (see Fig. 8) can be qualitatively described in the framework of the one-fluid

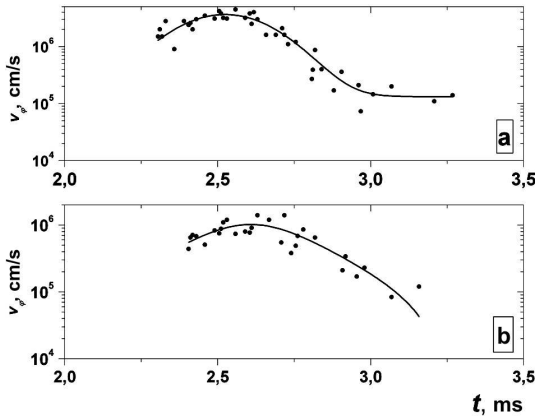

Fig. 7. Time dependences of the rotational velocity for plasma layers with $N_p = 1.7 \times 10^{13}$ (a) and 6.5×10^{13} cm^{-3} (b) for a mixture Ar + Ti ($p = 0.8$ Pa, $U_{\text{dis}} = 3.8$ kV, and $U_{\text{B}} = 2$ kV)

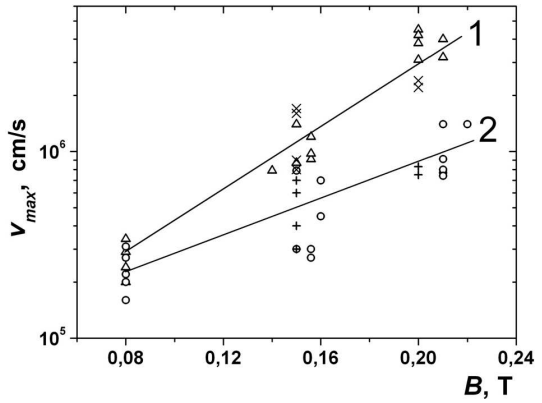

Fig. 8. Dependences of the maximum rotational velocity of plasma (Ar + Ti) layers with $N_p = 1.7 \times 10^{13}$ (1,△, ×) and 6.5×10^{13} cm^{-3} (2,○, +) on the magnetic field induction. $p =$ = 0.8 Pa, $U_{\text{dis}} = 3.8$ kV, △ and ○ are experimental data, × and + correspond to calculation results

MHD plasma model. As is seen from Eq. (15), the radial component j_r of the current density, when interacting with the longitudinal magnetic field B_z, stimulates the plasma rotation. In the first approximation, the rotational velocity v_φ is proportional to $j_r B_z$. Then it follows that the rotational velocity also increases with the magnetic field. The rotational velocity can be evaluated from the relation $v_\varphi = -BQ(t)/2\pi r\rho$, where the quantity $Q(t) = \int_0^t 2\pi r j_r dt$ was obtained in work [26] within the one-fluid MHD model. The results of our calculations are shown in Fig. 8. One can see that they are in satisfactory agreement with experimental results.

On the basis of experimental data, the magnitude of radial electric field in plasma can be evaluated using formula (5). The calculations give the E_r-values in the intervals of 1.6–90 and 1.3–28 V/cm for layers **A** and **B**, respectively, in the examined range of magnetic fields. Making allowance for the pressure gradient (formula (12)) gives a value for the radial electric field that is slightly lower. As was mentioned above, the rotational velocities of electrons and ions have to be different. Knowing the electric field, one can evaluate the rotational velocity for the ionic component by formula (4). The values calculated for Ar and Ti ions at $B = 0.08 \div 0.2$ T lie in the interval $(1.1 \div 9) \times 10^5$ cm/s for both plasma layers (at $B = 0.2$ T, the rotational velocities in layer **A** equal $(1.7 \div 2) \times 10^6$ cm/s). Those values of rotational velocity for the ionic component are a bit lower or close to the critical velocity $v_{\rm cr} = (2e\phi_i/m_i)^{1/2}$, where ϕ_i is the atomic ionization potential [27]. For argon, this quantity equals $v_{\rm cr} = 8.7 \times 10^5$ cm/s. On the other hand, the examined plasma has two basic ionic components (Ar and Ti), the critical velocities of which are different. For instance, $v_{\rm cr} = 5.2 \times 10^5$ cm/s for Ti. According to the results of work [28], the critical velocity for a two-component mixture can be determined from the relation $v_{\rm cr} = \sqrt{\frac{2(\alpha e\phi_{i1} + (1-\alpha)e\phi_{i2})}{\alpha m_{i1} + (1-\alpha)m_{i2}}}$, where ϕ_{i1} and ϕ_{i2} are the corresponding ionization potentials for atoms in the mixture, m_{i1} and m_{i1} are their masses, and α is the content of component 1 in the mixture. The calculated value is in satisfactory agreement with the experimental values of $v_{\rm cr}$ obtained for various mixtures [28]. The evaluation for the two-component mixture of neutral Ar and Ti atoms with their content of 1:1 gives the value $v_{\rm cr} = 7 \times 10^5$ cm/s. This estimate is quite correct in the case where the mixture with the given content is in the discharge volume before the discharge is initiated (before the plasma formation).

According to the conditions of the described experiment, Ti atoms are introduced in the direction along the column of the previously created Ar plasma (see Fig. 2), where they become ionized owing to their collisions with electrons (for Ti, the ionization potential is lower and the ionization rates are higher than those for Ar), ions (non-resonant charge exchange), and excited Ar atoms (Penning ionization). Then, it follows that the content of neutral titanium atoms in the main plasma column is insignificant. At 90% Ar + 10% Ti, the value $v_{\rm cr} = 8.4 \times 10^5$ cm/s, which is close to $v_{\rm cr}$ for argon. On the other hand, we may suppose that a high content of titanium atoms is characteristic of the regions near the cathodes. In this case, the law of isorotation (Ferraro's theorem) has to be taken into account, which reads that, for a stationary motion, the angular velocity is constant along the magnetic field lines. If the magnetic field has mirror geometry and the isorotation is present, the maximum velocity equals $v_{\rm max} = v_{\rm cr} R^{1/2}$, where R is the mirror ratio [7]. Taking this reasoning into account and adopting $v_{\rm cr} = 7 \times 10^5$ cm/s, we obtain that $v_{\rm max} \approx 8 \times 10^5$ cm/s, which is close to the value of $v_{\rm cr}$ for argon. Hence, as follows from the consideration given above and the estimations made in the general case, the rotational velocities of the ionic component are lower or close to the critical value for argon.

6. Conclusions

1. A specific feature of this work is the application of two-frequency microwave fluctuation reflectometry for the determination of the rotational velocity of plasma layers with different densities.

2. The difference between the angular rotational velocities of plasma layers with different densities ($\omega_\varphi^{\mathbf{A}} \neq \omega_\varphi^{\mathbf{B}}$) has been detected experimentally. The time dependences of rotational velocities for plasma layers with different densities are determined. The maximum of rotational velocity is achieved in 0.5 ms after the discharge has begun. The reflectometric measurements have confirmed the axial symmetry of the plasma column.

3. The rotational velocity of plasma layers is found to grow with the magnetic field in the examined interval of its values. The estimates obtained for the

rotational velocity in the framework of the one-fluid MHD model are in satisfactory agreement with experimental results.

4. On the basis of experimental data, the radial electric field strength in the plasma layers with various densities is evaluated. We obtain $E_r = 90$ V/cm at $N_p = 1.7 \times 10^{13}$ cm^{-3} and $E_r = 28$ V/cm at $N_p = 6.5 \times 10^{13}$ cm^{-3}.

1. K. Boyer, J.E. Hammel, C.L. Longmire *et al.*, in *Proceedings of the Second United Nations International Conference on the Peaceful Uses of Atomic Energy* (1958), Vol. 31, p. 319.
2. O.A. Anderson, W.R. Baker, A. Bratenahl *et al.*, in *Proceedings of the Second United Nations International Conference on the Peaceful Uses of Atomic Energy* (1958), Vol. 32, p. 155.
3. B. Lehnert, Nucl. Fusion **11**, 485 (1971).
4. C.E.S. Phillips, Proc. R. Soc. London, Sect. A **64**, 172 (1898).
5. A.W. Hull, Phys. Rev. **18**, 31 (1921).
6. F.M. Penning, Physica **4**, 71 (1937).
7. I.C. Teodorescu, R. Clary, R.F. Ellis *et al.*, Phys. Plasmas **17**, 052503 (2010).
8. B.M. Annaratone, A. Escarguel, T. Lefevre *et al.*, Phys. Plasmas **18**, 032108 (2011).
9. P.M. Valanjua, S.M. Mahajan, and H.J. Quevedo, Phys. Plasmas **13**, 062105 (2006).
10. E. Thomas, A. Eadon, and A. Edwynn, Phys. Plasmas **12**, 042109 (2005).
11. A.B. Mikhailovskii, Dzh.G. Lominadze, A.P. Churikov, and V.D. Pustovitov, Fiz. Plazmy **35**, 307 (2009).
12. V.V. Dolgopolov, V.L. Sizonenko, and K.N. Stepanov, Ukr. Fiz. Zh. **18**, 18 (1973).
13. V.M. Zhdanov, *Transport Processes in Multicomponent Plasma* (Taylor and Francis, New York, 2002).
14. L.I. Romanyuk and V.M. Slobodyan, Ukr. Fiz. Zh. **17**, 2004 (1972).
15. N.P. Efremov and N.P. Poluektov, J. Phys. D **31**, 988 (1998).
16. E. Del Bosco, S.W. Simpsont, R.S. Dallaqua, A. Montes, J. Phys. D **24**, 2008 (1991).
17. Yu.V. Kovtun, A.I. Skibenko, E.I. Skibenko *et al.*, Vopr. At. Nauki Tekhn. **68**, 214 (2010).
18. Yu.V. Kovtun, A.I. Skibenko, E.I. Skibenko *et al.*, Plasma Phys. Rep. **36**, 1065 (2010).
19. Yu.V. Kovtun, A.I. Skibenko, E.I. Skibenko *et al.*, Ukr. Fiz. Zh. **55**, 1269 (2010).
20. E.I. Skibenko, Yu.V. Kovtun, A.I. Skibenko *et al.*, Techn. Phys. **56**, 623 (2011).
21. E.I. Skibenko, Yu.V. Kovtun, A.I. Skibenko, V.B. Yuferov, Patent Ukraine 38780, Publ. 12.01.2009, Bul. No. 1 (2009).
22. L.D. Landau and E.M. Lifshitz, *Mechanics* (Butterworth Heinemann, Oxford, 2001).
23. L.D. Landau and E.M. Lifshits, *The Classical Theory of Fields* (Pergamon Press, Oxford, 1983).
24. H. Alfvén and C.-G. Fälthammar, *Cosmical Electrodynamics: Fundamental Principles* (Clarendon Press, Oxford, 1963).
25. E.Z. Gusakov and A.Yu. Popov, in *Abstracts of the 31st European Physical Society Conference on Plasma Physics, London, 2004* (European Physical Society, 2004), Vol. 28G, p. 1.181.
26. B. Lehnert, Nucl. Fusion **1**, 125 (1961).
27. H. Alfvén and G. Arrhenius, *Evolution of the Solar System* (NASA, Washington, DC, 1976).
28. I. Axnas, Astrophys. Space Sci. **55**, 139 (1978).

Received 17.07.12.
Translated from Ukrainian by O.I. Voitenko

Ю.В. Ковтун, Є.І. Скібенко,
А.І. Скибенко, В.Б. Юферов

ДОСЛІДЖЕННЯ ОБЕРТАННЯ
ПЛАЗМОВИХ ШАРІВ РІЗНОЇ ГУСТИНИ
В СХРЕЩЕННИХ $\mathbf{E} \times \mathbf{B}$ ПОЛЯХ

Р е з ю м е

Робота присвячена визначенню швидкості обертання плазмових шарів різної густини у плазмі імпульсного відбивного розряду. Для цього була запропонована і використовувалась двочастотна НВЧ флуктуаційна рефлектометрія. За її допомогою було встановлено відмінність кутових швидкостей обертання плазмових шарів різної густини та визначено їх часовий хід. Також встановлено, що швидкість обертання плазмових шарів зростає із збільшенням індукції магнітного поля. На основі одержаних експериментальних даних оцінена величина напруженості радіального електричного поля в плазмових шарах різної густини.